

Electronic Interactions in a New π -Extended Tetrathiafulvalene Dimer

Marta C. Díaz,^[a] Beatriz M. Illescas,^[a] Nazario Martín,^{*[a]} Igor F. Perepichka,^[b, e] Martin R. Bryce,^{*[b]} Eric Levillain,^{*[c]} Rafael Viruela,^[d] and Enrique Ortí^{*[d]}

Dedicated to Professor Jan Becher on the occasion of his retirement and in recognition of his outstanding achievements to tetrathiafulvalene chemistry

Abstract: The first π -extended tetrathiafulvalene (exTTF) dimer in which the two exTTF units are covalently connected by 1,3-dithiole rings has been obtained in a multistep synthetic procedure involving the Ullmann cross-coupling reaction by using copper(I) thiophene-2-carboxylate (CuTC). The electronic spectrum reveals a significant electronic interaction between the exTTF units. The electrochemical study carried out by cyclic voltammetry in so-

lution and in thin-layer conditions, and the electrochemical simulation and spectroelectrochemical (SEC) measurements confirm the electronic communication and show that the oxidation of dimer **14** occurs as two consecutive $2e^-$

processes $D^0-D^0 \rightarrow D^{2+}-D^0 \rightarrow D^{2+}-D^{2+}$. Theoretical calculations, performed at the B3P86/6-31G* level, confirm the experimental findings and predict that **14**²⁺ exists as a delocalized $D^{+}-D^{+}$ species in the gas phase and as a localized $D^{2+}-D^0$ species in solution (CH₃CN or CH₂Cl₂). Oxidation of **14**²⁺ forms the tetracation **14**⁴⁺ which is constituted by two aromatic anthracene units bearing four aromatic, almost orthogonal 1,3-dithiolium cations.

Keywords: cyclic voltammetry • density functional calculations • electron donors • spectroelectrochemistry • tetrathiafulvalenes

Introduction

Tetrathiafulvalene (TTF) derivatives with extended π conjugation are an important class of electron-donor systems. They present remarkable differences in comparison to the parent TTF in terms of oxidation potential values, geometry, and charge delocalization, making them versatile building blocks in supramolecular and materials chemistry.^[1] Of particular interest are the extended TTF derivatives bearing a

p-quinodimethane central spacer (**1**, **2**), which oxidize at lower potential values owing to charge delocalization and to the decrease of the intramolecular on-site Coulombic repulsion.^[2] In contrast to parent TTF, which forms stable radical cation and dication states, *p*-quinodimethane analogues of TTF (exTTF, **2**) are characterized by a single, two-electron oxidation wave in the cyclic voltammogram (CV) to yield thermodynamically stable dications ($E_{ox} = 0.40$ V, R = H, vs. Ag/AgCl). exTTFs possess a saddle-shaped structure in the


[a] Dr. M. C. Díaz, Dr. B. M. Illescas, Prof. N. Martín
Departamento de Química Orgánica
Facultad de Ciencias Químicas, Universidad Complutense
28040 Madrid (Spain)
Fax: (+34)91-394-4103
E-mail: nazmar@quim.ucm.es

[b] Dr. I. F. Perepichka, Prof. M. R. Bryce
Department of Chemistry and
Centre for Molecular and Nanoscale Electronics
University of Durham, Durham DH1 3LE (UK)
Fax: (+44)191-384-4737
E-mail: m.r.bryce@durham.ac.uk

[c] Dr. E. Levillain
Chimie, Ingénierie Moléculaire et Matériaux d'Angers (CIMMA)
CNRS UMR 6200, 2, bd. Lavoisier, 49045 Angers Cedex (France)
Fax: (+33)241-735-405
E-mail: eric.levillain@univ-angers.fr

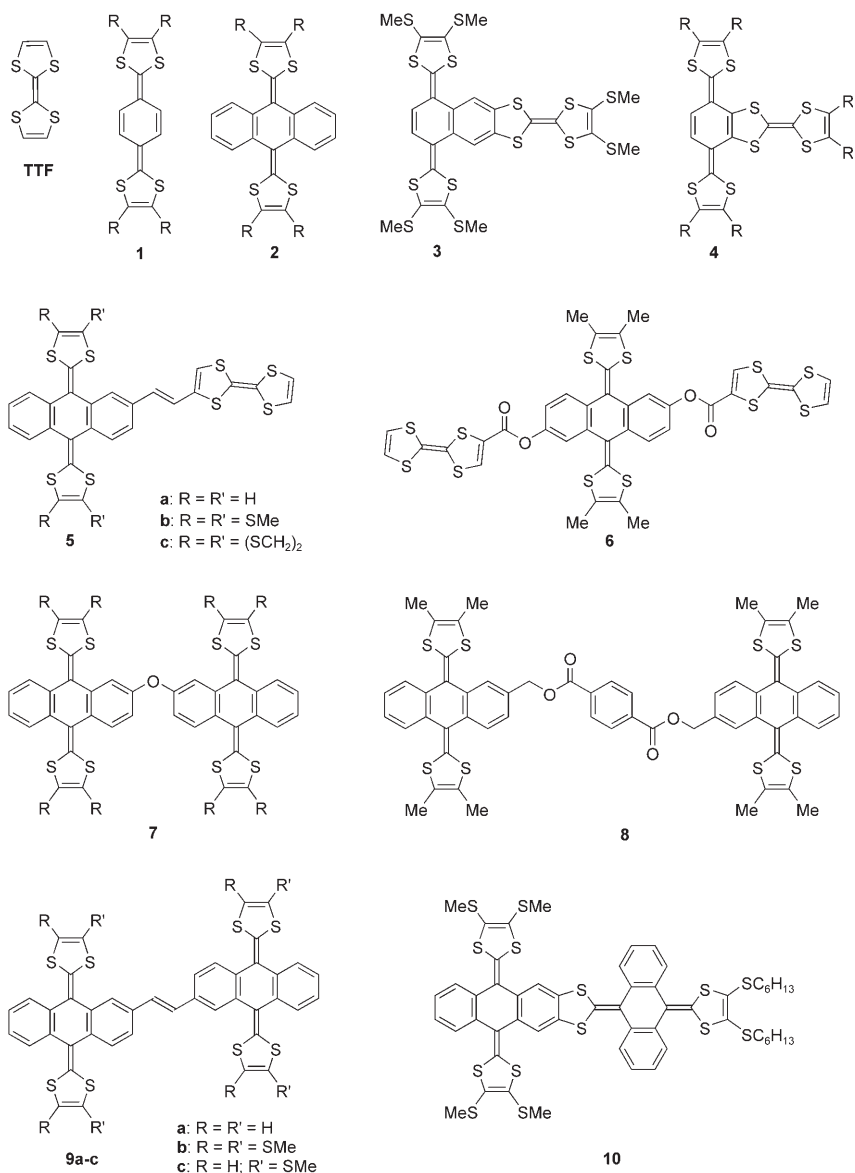
[d] Dr. R. Viruela, Dr. E. Ortí
Institut de Ciència Molecular
Universitat de València
46100 Burjassot, València (Spain)
Fax: (+34)96-354-3156
E-mail: enrique.orti@uv.es

[e] Dr. I. F. Perepichka
On leave from L. M. Litvinenko Institute of Physical Organic and Coal Chemistry, National Academy of Sciences of Ukraine, Donetsk 83114 (Ukraine)

 Supporting information for this article (cyclic voltammetry and spectroelectrochemistry data for compounds **12** and **14**) is available on the WWW under <http://www.chemeurj.org/> or from the authors.

neutral state, owing to the steric hindrance caused by benzoannulation of the quinoid moiety; this structure shape contrasts with the almost planar structure of the TTF moiety. A dramatic structural change accompanies the oxidation to the dication; the central anthracene moiety becomes aromatic and planar and the 1,3-dithiolium cations lie orthogonal to the anthracene plane.^[3]

Quinoid π -extended TTFs have received special attention as materials with increased dimensionality^[2] and nonlinear optical (NLO) properties.^[4] We have recently found that exTTF derivatives covalently attached to the electron acceptor [60]fullerene dramatically enhance the stability of the charge-separated excited state in the preparation of artificial photosynthetic systems.^[5] The importance of these π -extended bis(1,3-dithiole) compounds has led to systematic studies of their chemical functionalization at both the anthracene^[6] and dithiole units,^[7] which has enabled the preparation of more sophisticated electron-donor TTF derivatives and novel electroactive donor-acceptor systems.^[8] Compounds **3**,^[9] **4**,^[10] **5**,^[11] and **6**^[6] are rep-



Abstract in Spanish: *Se ha sintetizado el primer dímero derivado de TTF π -extendido (exTTF) en el que las dos unidades de exTTF se encuentran unidas mediante un enlace covalente a través de los anillos de 1,3-ditiol. El procedimiento sintético consta de varios pasos e implica una reacción de acoplamiento cruzado de tipo Ullmann empleando 2-tiofencarboxilato de cobre(I) (CuTC). Los espectros electrónicos revelan una interacción electrónica significativa entre las unidades de exTTF. Se ha realizado el estudio electroquímico mediante voltamperometría cíclica en disolución y en condiciones de capa fina, así como la simulación electroquímica y las medidas espectroelectroquímicas. Los datos obtenidos confirman la comunicación electrónica entre ambas unidades, y muestran que la oxidación del dímero **14** ocurre como dos procesos que involucran dos electrones $D^0-D^0 \rightarrow D^{2+}-D^0 \rightarrow D^{2+}-D^{2+}$. Cálculos teóricos B3P86/6-31G* confirman los hechos experimentales y predicen que **14**²⁺ existe como una especie deslocalizada $D^{2+}-D^{2+}$ en fase gas y como una especie localizada $D^{2+}-sD^0$ en disolución (CH_3CN o CH_2Cl_2). La oxidación de **14**²⁺ forma la especie tetracatiónica **14**⁴⁺, constituida por dos unidades de antraceno aromáticas con cuatro cationes 1,3-ditiolio aromáticos en disposición prácticamente ortogonal a las unidades de antraceno.*

resentative examples of combined TTF-exTTF systems, which possess multistage redox behavior.

In contrast to the large number of studies on bis- and multi-TTF derivatives,^[12] there are only a few recent examples of dimeric exTTF derivatives with quinoid structures, namely **7**,^[13] **8**,^[14] **9**,^[15] and **10**.^[16] These molecules have been studied in the search for new and more sophisticated π -extended systems as strong donors and as molecules for fundamental studies of intramolecular electronic interactions. In systems **7-9** the linkage involves the anthracene moieties of both exTTFs and no intramolecular electronic interaction was observed (electrochemical evidence), indicating that these dimers behave as two independent exTTF units with no effective conjugation between them. Compound **10** is the only example to date of an anthracene-dithiole ring fusion. The CV of compound **10** shows two, two-electron oxidation waves corresponding to the sequential formation of **10**²⁺ and **10**⁴⁺ ($\Delta E_{ox} = 130$ mV). This difference in E_{ox} values

could not be readily explained by the different substitution pattern of the two exTTF units. It is therefore considered to be due to a significant intramolecular electronic interaction through the conjugated system, that is, the dication formed in the initial process raises the oxidation potential of its partner exTTF unit.

These findings prompted us to synthesize and investigate the electronic interactions of the new dimeric donor system **14**, in which the two exTTF units are directly linked through the 1,3-dithiole rings by means of a single bond. The synthesis of dimer **14** requires a different synthetic approach involving the initial functionalization of the 1,3-dithiole ring in the exTTF molecule. To determine the electronic interaction between both exTTF units, thorough chemical oxidation titration, electrochemical, and spectroelectrochemical (SEC) studies have been performed. In addition, to gain a better understanding of the structural and electronic properties of the novel dimer, theoretical calculations at the B3P86/6-31G* level have been performed on compound **14**.

Results and Discussion

Synthesis: The preparation of the target compound **14** was accomplished, as depicted in Scheme 1, by self-coupling of the iodo-exTTF derivative **13**. The known starting material, trimethylsubstituted exTTF **12**, was obtained in seven steps from commercially available anthrone **11**.^[7a] Lithiation of **12** using lithium diisopropylamide (LDA) in dry tetrahydrofuran (THF) at -78°C followed by iodination with perfluorohexyl iodide (PFHI)^[17] afforded **13** as a stable yellow solid in 83% yield. Conversion of **13** into the exTTF dimer **14** was achieved by means of the Ullmann coupling using copper(i) thiophene-2-carboxylate (CuTC) in 1-methylpyrrolidin-2-one at 20°C . CuTC was freshly prepared from 2-thio-

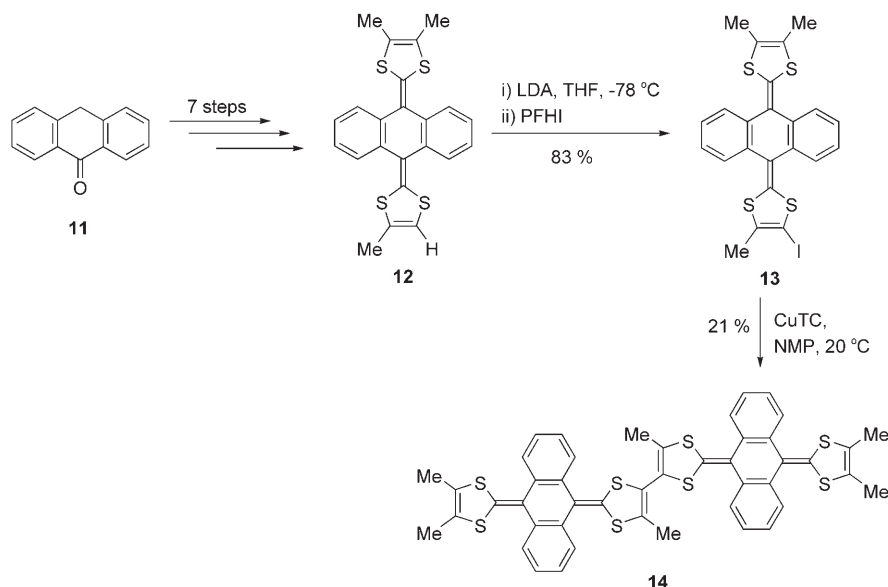
phencarboxylic acid and copper(i) oxide by refluxing in toluene.^[18] Under these conditions, dimer **14** was obtained as a stable yellow solid in 21% yield. It is interesting to note that in addition to the presence of unreacted compound **13**, compound **12**, resulting from the loss of iodine from **13**, was also formed in the reaction, thus accounting for the moderate yield of **14**.

The structure of the dimeric donor **14** was confirmed by analytical and spectroscopic data. Thus, the ^1H NMR spectrum shows, in addition to the presence of the aromatic protons, the methyl groups at $\delta=1.93$ (s, 12H) and 1.90 (s, 6H). The ^{13}C NMR spectrum reveals the presence of the aromatic carbons at $\delta\sim 110\text{--}135$ and the methyl carbons at $\delta\sim 15$. The MS of **14** exhibits a low-intensity molecular ion [M^+ , 8%], and the base peak at m/z 421 (100%), which could correspond to either the monomeric fragment or to the doubly charged molecular ion ($[M^{2+}]$).

UV/Vis spectra: The UV/Vis spectrum of **14** is presented together with those of its precursors **12** and **13** in Figure 1. The electronic spectra of these compounds show a most significant absorption band at $\lambda_{\text{max}}\sim 440$ nm, which explains their yellow color in solution. This band was previously assigned to an intramolecular electron transfer process from the 1,3-dithiol-2-ylidene units to the hydrocarbon skeleton for laterally benzoannulated exTTFs.^[3] Interestingly the λ_{max} value for **14** (442 nm) is slightly red-shifted in comparison with its precursors **12** (435 nm) and **13** (437 nm), this shift suggests some electronic interaction between both exTTF units in the dimer.

Cyclic voltammetry (CV): The CV of compound **12** in acetonitrile (AN) shows typical behavior observed for exTTF donors.^[3,11] A single, two-electron, quasireversible oxidation $\text{D}^0\rightarrow\text{D}^{2+}$ is registered (Figures 2 and S1 and Table S1 in the Supporting Information). The difference between the anodic and the cathodic peaks increases with scan rate, the values increase from 224 to 348 mV at scan rates of 20 and 500 mV s^{-1} , respectively. The large separation between the anodic and cathodic peaks is due to the major conformational change that accompanies the electron-transfer process. It is a typical example of inverted potentials in a two-electron process; that is, it is easier to remove the second electron than the first.^[19] In such a process, it is very difficult to detect the radical cation $\text{D}^{\cdot+}$.

For compound **14** with two exTTF units, two closely spaced oxidation peaks are observed in the CV (Figure 3 and Figure S2



Scheme 1.

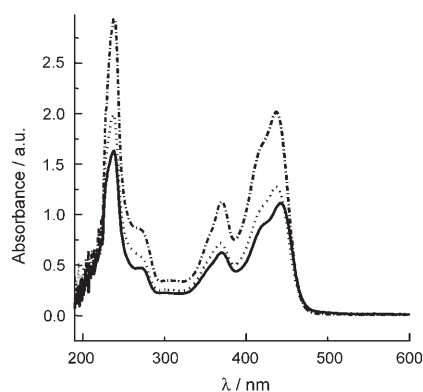


Figure 1. UV/Vis spectra of compounds **12** (.....), **13** (----), and **14** (—) in CH_2Cl_2 at 20°C .

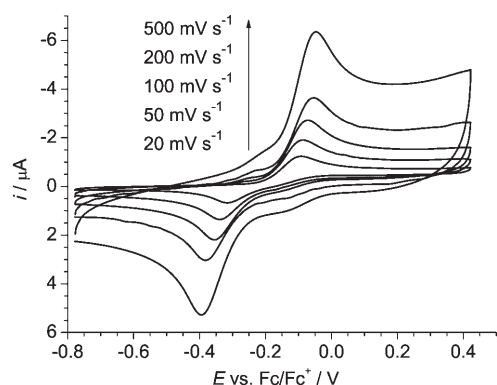


Figure 2. CVs of compound **12** in AN and $0.1\text{ M Bu}_4\text{NPF}_6$ at different scan rates; CVs recorded at 20°C .

in the Supporting Information); these peaks can be attributed to consecutive oxidations of the first and second exTTF moieties ($\text{D}^0\text{-D}^0 \rightarrow \text{D}^{2+}\text{-D}^0 \rightarrow \text{D}^{2+}\text{-D}^{2+}$), respectively. Owing to the low solubility of compound **14** in AN, the oxidation is complicated by adsorption processes on the electrode surface (Figure S2 in the Supporting Information). Therefore, we performed further CV studies in a mixture of AN:di-

chloromethane (DCM), 1:1 v/v, in which two overlapping anodic peaks on oxidation and two cathodic peaks on re-reduction were observed at different scan rates (from 100 to 2000 mV s^{-1}) (Figure 4 and Figure S3 in the Supporting Information). The deconvoluted CV for compound **14** at a scan rate of 100 mV s^{-1} (Figure 3b) clearly shows two con-

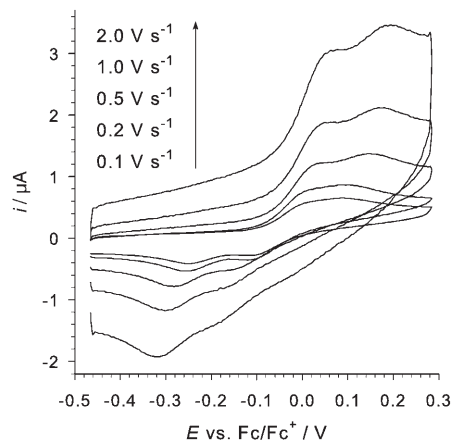


Figure 4. CV of compound **14** in AN:DCM (1:1 v/v), $0.25\text{ M Bu}_4\text{NPF}_6$ at different scan rates under diffusion conditions.

secutive oxidation and two re-reduction processes. Large differences in the potential of the anodic and cathodic peaks on the deconvoluted CV for both processes ($E_{\text{pa}} = -0.020$ and $+0.075\text{ V}$, $E_{\text{pc}} = -0.225$ and $-0.080\text{ V vs. Fc/Fc}^+$) indicate that they are both substantially electrochemically irreversible.

Thin-layer cyclic voltammetry (TLCV) experiments performed at very low scan rates of 2 and 5 mV s^{-1} provide a cleaner separation of the first ($\text{D}^0\text{-D}^0 \rightarrow \text{D}^{2+}\text{-D}^0$; $E_{\text{pa}} = -0.09\text{ V vs. Fc/Fc}^+$) and second ($\text{D}^{2+}\text{-D}^0 \rightarrow \text{D}^{2+}\text{-D}^{2+}$; $E_{\text{pa}} = 0.00\text{ V}$) oxidation processes (Figure 5 and Figure S4 in the Supporting Information). The difference in oxidation potentials for the first and the second exTTF moieties indicates that they interact electronically. Consequently, the oxidation

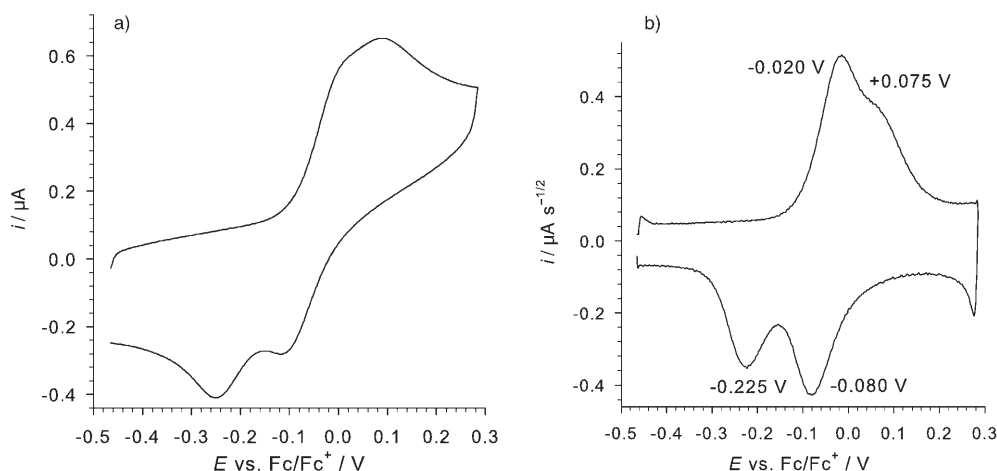


Figure 3. CV of compound **14** in AN:DCM (1:1 v/v), $0.25\text{ M Bu}_4\text{NPF}_6$ at 100 mV s^{-1} (a) and deconvoluted CV (b).

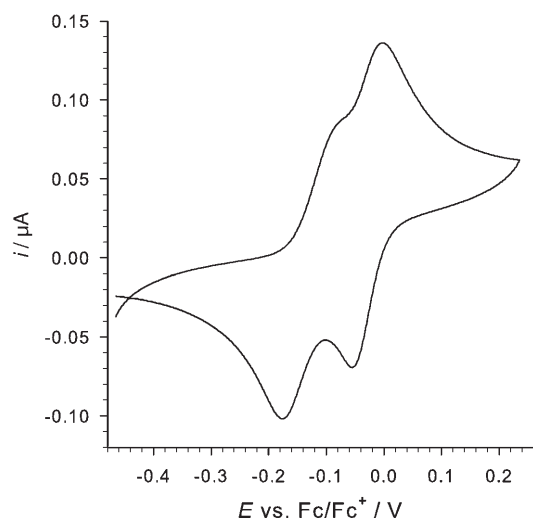
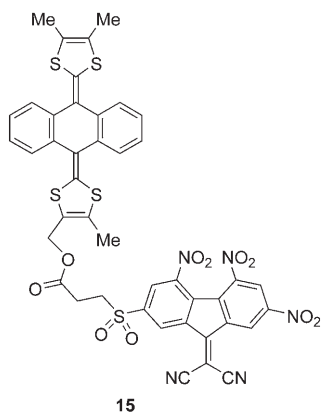


Figure 5. TLCV of compound **14** in AN:DCM, 1:1 v/v and 0.25 M Bu₄NPF₆ at a scan rate of 2 mV s⁻¹.

of the first moiety shifts the oxidation potential of its partner to more positive potentials (for TLCV, the shift at a scan rate of 2 mV s⁻¹ is ~100 mV). This is similar to that observed for compound **10**, as discussed above in the Introduction.

Spectroelectrochemistry: Generally for exTTF systems the two-electron oxidation process ($D^0 \rightarrow D^{2+}$) is driven by the gain in aromatization energy at the $D^{+} \rightarrow D^{2+}$ step.^[3] The radical-cation species D^{+} are not registered in the CV or SEC experiments, and solutions are EPR-silent during the oxidation process.^[8b] For molecule **15**, which comprises the 2e exTTF donor and the 1e nitrofluorene acceptor moiety, intermolecular donor–acceptor interactions resulted in an EPR signal from only the acceptor radical anion, and



simultaneous electrochemistry and EPR (SEPR) experiments for compound **15** did not produce an EPR signal for D^{+} .^[8b] Fast radiative techniques, for example, flash photolysis, are required for the detection of the transient radical cations D^{+} of exTTF systems (half-life times are in the range of tens of microseconds to tens of milliseconds), which rapidly disproportionate into D^0 and D^{2+} species.^[20,5f]

Nonetheless, the two separate oxidation waves in the CVs of compound **14** (Figures 3–5) could be alternatively interpreted as two, consecutive, single-electron processes on each exTTF moiety ($D^0 \rightarrow D^{+} \rightarrow D^{2+} \rightarrow D^{2+} \rightarrow D^{2+}$), which do not interact electronically with each other. Although this seems a less-probable scenario, we decided to perform SEC studies to provide additional information about the mechanism of the electrochemical oxidation process of compound **14**. Electrochemical oxidation of compound **12** ($D^0 \rightarrow D^{2+}$) in an acetonitrile solution results in a decrease of the absorption at 431 nm, characteristic of the neutral state, and the appearance of a new, broad band at about 460–520 nm, diagnostic of the dication species of exTTF donors,^[20a,b] with a sharp isosbestic point at 460 nm (Figure 6a). Very similar evolution of the spectra is observed upon oxidation of compound **14** in SEC experiments, that is, a decrease of the band at

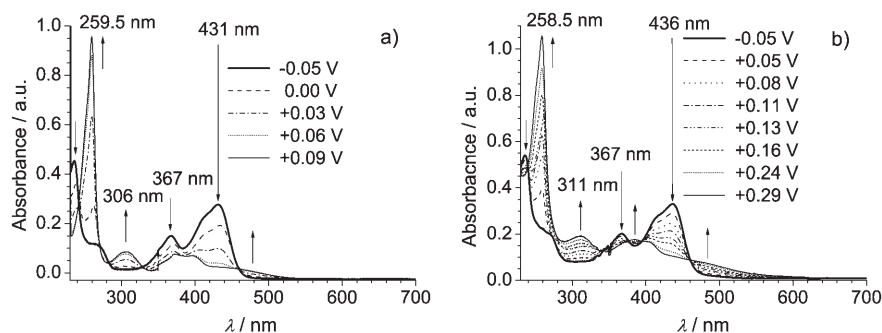


Figure 6. SEC of compounds **12** (a) and **14** (b) in AN, 0.1 M Bu₄NPF₆ (1 mm quartz cell, transmission mode). Potentials are quoted vs. Pt wire.

436 nm and the appearance of new band at about 460–540 nm with an isosbestic point at 460 nm (Figure 6b). No low-energy bands in the 600–700 nm region, in which an absorption of the radical cation is expected,^[20] were observed in either case. Clean isosbestic points in the SEC measurements of compound **14** over the range of potentials from -0.05 to $+0.29$ V versus Pt wire ($D^0 \rightarrow D^0 \rightarrow D^{2+} \rightarrow D^0 \rightarrow D^{2+} \rightarrow D^{2+}$) could indicate that the intermediate species $D^{2+} \rightarrow D^0$ retains characteristic absorptions of both neutral and oxidized exTTF in the electronic spectrum, from the D^0 and D^{2+} parts of the molecule, respectively.

The same spectral changes for compounds **12** and **14** were also observed in SEC experiments in DCM, thus confirming that in this low-polar solvent the oxidation of **14** also occurs as two-electron processes to yield $D^{2+} \rightarrow D^0$ and then $D^{2+} \rightarrow D^{2+}$ species (see Figure S5a,b in the Supporting Information).

Very similar results were obtained in SEC studies of compound **14** in AN:DCM, 1:1 v/v in a cell with true thin-layer conditions (125 μm) (Figure 7). Analysis of a 2D map of the SEC data (Figure 7a) shows that in the potential range of 0.3–0.5 V, in which the $\text{D}^{2+}\text{--D}^0$ species exists, the bands characteristic for the neutral state of **14** (367 and 436 nm) remained observable although their intensities decreased compared to the initial spectrum of **14** because only one exTTF moiety remains uncharged. These bands disappear for the 14^{4+} state.

Thus, all these data indicate that the electrochemical oxidation of compound **14** occurs as two consecutive 2e processes $\text{D}^0\text{--D}^0 \rightarrow \text{D}^{2+}\text{--D}^0 \rightarrow \text{D}^{2+}\text{--D}^{2+}$.

Chemical oxidation of compounds 12 and 14: We also performed chemical oxidative titration of compounds **12** and **14** by using NOSbF_6 in AN monitored by electron absorption

spectrophotometry. Similar to the SEC experiments, chemical oxidation leads to a decrease of the characteristic absorption of the neutral compounds **12** (366 and 430 nm) and **14** (366 and 435 nm) and to the appearance of dication bands at about 460–530 nm with clean isosbestic points at 327 and 462 nm and at 336 and 463 nm, respectively (Figure 8). Similar to SEC experiments, no absorption in the long wavelength/near-IR region, characteristic of the radical cations, was observed in either case (Figure 8a and b).

Electrochemical simulation: Oxidation of compound **12** can be described by inverted potentials following Equations (1)–(3):

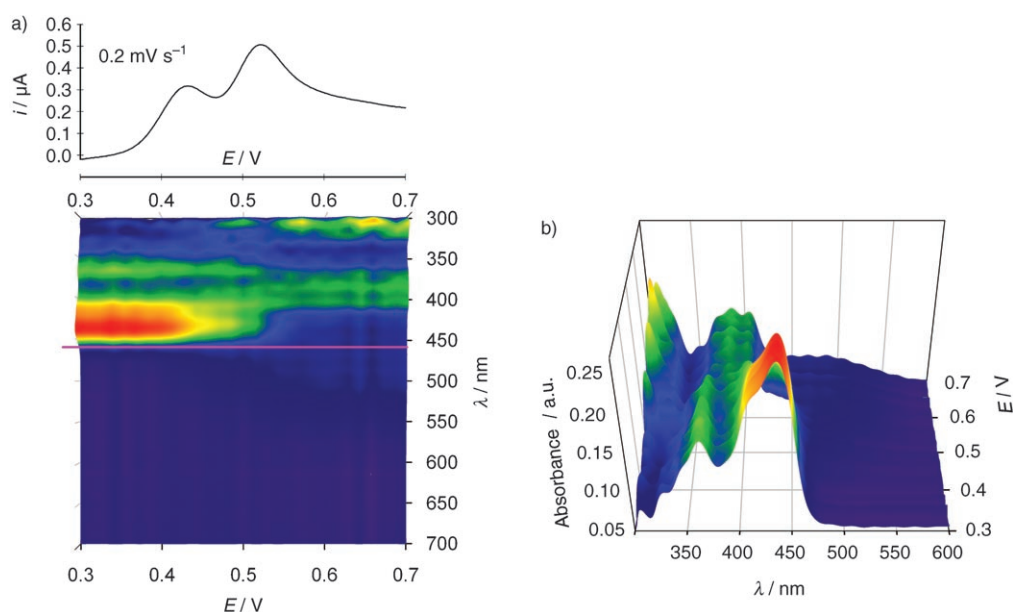
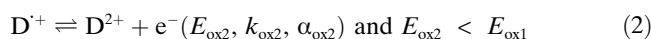
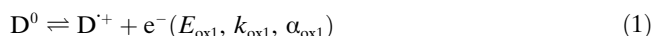


Figure 7. a) TL-CV (top) and 2D map of TL-SEC (bottom) experiment of compound **14** in AN:DCM, 1:1 v/v and 0.25 M Bu_4NPF_6 ; thin-layer conditions (125 μm , reflection mode). Potentials are quoted vs. Ag wire. The magenta line is an isosbestic point. b) 3D representation of the SEC data.

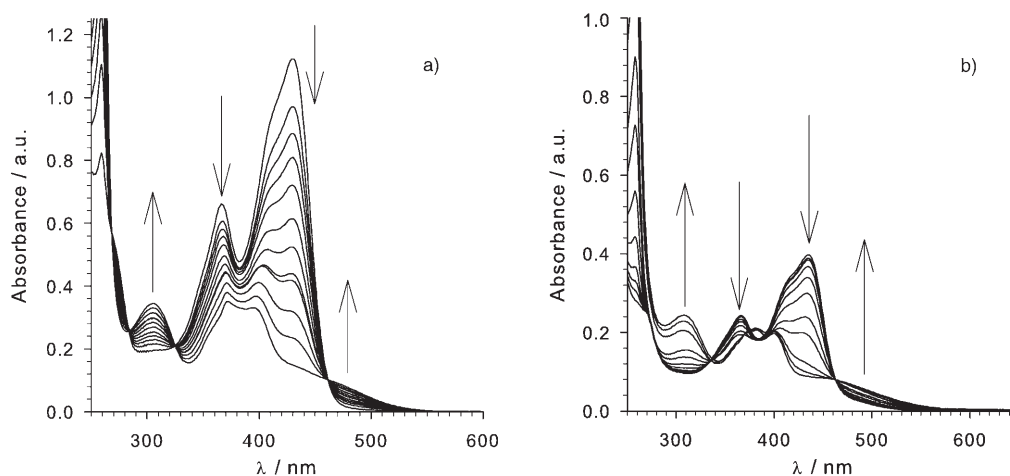


Figure 8. UV/Vis absorption spectra of compounds **12** (a) and **14** (b) upon titration with NOSbF_6 in AN. Arrows show the evolution of the bands when NOSbF_6 is added.



To validate this hypothesis, a quantitative analysis of the data over the scan-rate range investigated was carried out with the software package Digisim 3.05. Good simulation fits were found for scan rates from 0.1 to 5.0 V s⁻¹ at +20°C (Table 1 and Figure 9). Better fits were obtained at faster scan rates by the inclusion of the disproportionation reactions with $k_{1\text{disp}} = 10^6 \text{ M}^{-1} \text{ s}^{-1}$, although this does not provide an accurate assessment of this parameter (Table 1). Because the formal potential E^0 for the $D^{+} \rightarrow D^{2+}$ transformation

Table 1. Redox potentials and electron transfer parameters^[a] for compound **12** estimated by fitting with the software package Digisim 3.05.

$D^{[b]}$ [cm ² s ⁻¹]		D ²⁺ /D ⁺	D ⁺ /D ⁰
4.3×10^{-6}	E^0 [V]	-0.34	-0.18
	α	0.60	0.35
	$k^{[b]}$ [cm s ⁻¹]	5.0×10^{-3}	5.0×10^{-3}

[a] Potentials E^0 vs. Fc/Fc⁺; α is the electron-transfer coefficient; k is the electron-transfer rate constant. [b] D is the diffusion coefficient and k is the electron-transfer rate constants; their values were set the same for all redox states.

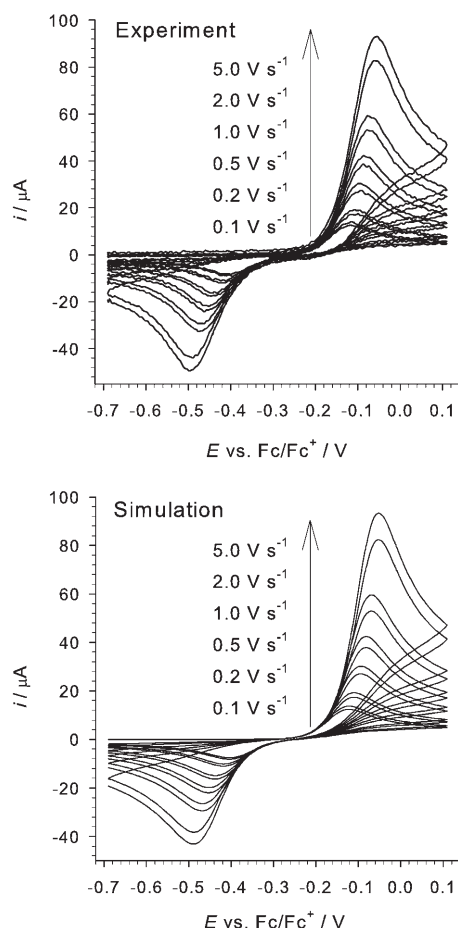
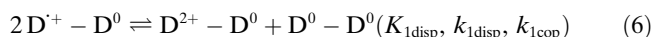
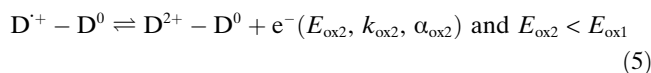
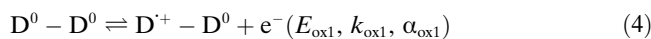


Figure 9. Experimental and simulated CVs for **12** (0.1 mM) in AN:DCM (1:1 v/v) and 0.25 M Bu₄NPF₆ at +20°C. The first two cycles have been shown for both experimental and simulated CVs.

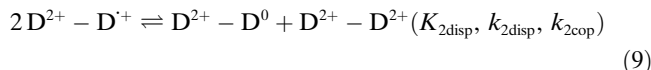
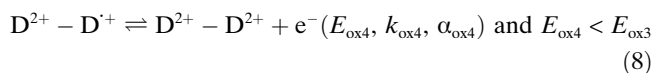
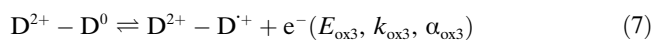
(-0.34 V) is lower than E^0 for $D^0 \rightarrow D^{+}$ (-0.19 V), the oxidation in the CV experiment occurs as a 2e process (Figures 2 and 9 and Table 1).

According to the experimental results (CV, SEC) and the electrochemical behavior of **12**, the oxidation of **14** can be described by two successive inverted potentials following Equations (4)–(9):

First process:



Second process:



As the two oxidation processes occur at very similar potentials, and the solubility of **14** is low in 0.25 M Bu₄NPF₆/AN:DCM (1:1 v/v) at +20°C (low current intensity), the electron-transfer coefficients (α), the electron-transfer rate constants (k), and the diffusion coefficients (D) were set the same for all the redox states. Good simulation fits were found for scan rates from 0.1 to 2.0 V s⁻¹ (Table 2 and

Table 2. Redox potentials and electron-transfer parameters^[a] for compound **14** estimated by fitting with the software package Digisim 3.05.

$D^{[b]}$ [cm ² s ⁻¹]		D ²⁺ -D ⁰ / D ⁺ -D ⁰	D ⁺ -D ⁰ / D ⁰ -D ⁰	D ²⁺ -D ²⁺ / D ⁺ -D ²⁺	D ⁺ -D ²⁺ / D ⁰ -D ²⁺
1.2×10^{-6}	E^0 [V ⁻¹]	-0.19	-0.10	-0.05	+0.01
	$\alpha^{[b]}$	0.5	0.5	0.5	0.5
	$k^{[b]}$ [cm ¹ s ⁻¹]	2.0×10^{-3}	2.0×10^{-3}	2.0×10^{-3}	2.0×10^{-3}

[a] Potentials E^0 vs. Fc/Fc⁺; D is the diffusion coefficient, α is the electron-transfer coefficient; k is the electron-transfer rate constant. [b] D , α , and k were set the same for all redox states.

Figure 10). Agreement was improved at faster scan rates by inclusion of the disproportionation reactions with $k_{1\text{disp}} = 10^6 \text{ M}^{-1} \text{ s}^{-1}$, although this does not provide an accurate assessment of this parameter (Table 2). With such an electrochemical process [$E^0(D^{+}-D^0 \rightarrow D^{2+}-D^0) < E^0(D^0-D^0 \rightarrow D^{+}-D^0)$ and $E^0(D^{+}-D^{2+} \rightarrow D^{2+}-D^{2+}) < E^0(D^0-D^{2+} \rightarrow D^{+}-D^{2+})$]; Table 2], the possibility of detecting the radical cations D^0-D^{+} or $D^{2+}-D^{+}$ is excluded on the timescale of usual electrochemical experiments. Thus, the oxidation of **14** can be interpreted by two consecutive inverted potentials on each exTTF moiety which are electronically interacting.

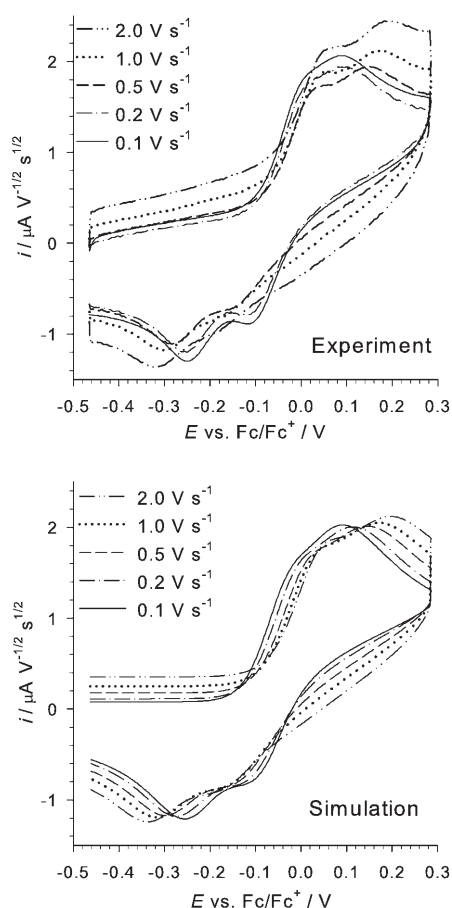


Figure 10. Experimental and simulated CVs for **14** (0.1 mM) in AN:DCM (1:1 v/v), 0.25 M Bu₄NPF₆ at +20 °C. Note that the CVs were normalized to V^{1/2}, in which V is the scan rate.

Theoretical calculations: To gain a deeper understanding of the experimental data, the molecular structures and the electronic properties of compounds **12** and **14** were theoretically investigated in both neutral and oxidized states. Compound **12** was studied as a reference system. Most of the calculations were performed within the density functional theory (DFT) approach by using the gradient-corrected B3P86 hybrid functional and the 6-31G* basis set (B3P86/6-31G*). DFT calculations include electron correlation effects at relatively low computational cost and are known to provide accurate equilibrium geometries.^[21]

Neutral compounds: The minimum-energy conformation of **12** corresponds to the butterfly-shaped structure depicted in Figure 11a. To relieve the short contacts between the sulfur

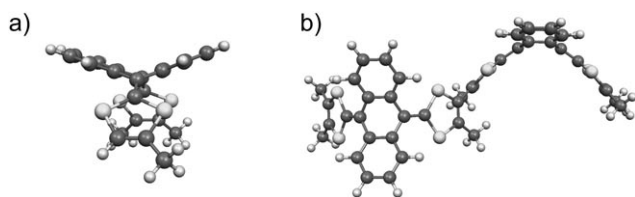


Figure 11. Minimum-energy B3P86/6-31G*-optimized conformations calculated for a) **12** and b) **14** (C₂ symmetry).

atoms and the hydrogen atoms in the *peri* positions, the central ring of the anthracene unit folds in a boat conformation and the molecule adopts a butterfly- or saddle-like structure, in which the benzene rings point upwards and the dithiolenyl rings point downwards. The conformation calculated for **12** is similar to that obtained for unsubstituted exTTF^[3,22] and is consistent with the crystal structures observed for different derivatives.^[2b,8d,20a,23]

Each exTTF unit in compound **14** adopts a butterfly structure similar to that predicted for **12**. The minimum-energy conformation corresponds to the C₂ structure depicted in Figure 11b. To alleviate the steric interactions between the exTTF units, the molecule is twisted by 105° around the central single bond linking the 1,3-dithiolenyl rings. The distortions from planarity of each exTTF fragment are described in terms of three angles. The anthracene systems are folded along the C9...C10 vectors (see Figure 12a for atom number-

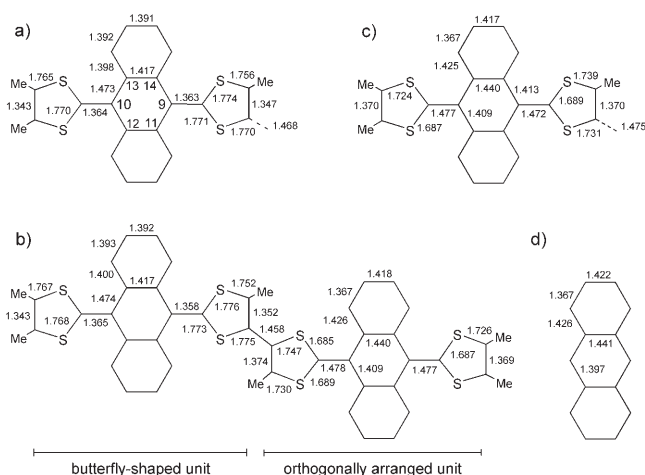


Figure 12. B3P86/6-31G*-optimized bond lengths (in Å) calculated for a) neutral molecule **14** (C₂ symmetry, atom numbering is given for the central ring), b) **14**²⁺ (no symmetry, in CH₃CN), c) **14**⁴⁺ (C₂ symmetry, in CH₃CN), and d) anthracene (D_{2h} symmetry). Only a half of the molecule is depicted for **14** and **14**⁴⁺. The lengths of chemically equivalent bonds that are identical (to the thousandth) are not given.

ing) by an angle of 38°. This value is identical to that calculated for monomer **12** and compares well with those experimentally found for exTTF derivatives (35–45°).^[2b,8d,20a,23] The dithiolenyl rings are tilted by 34° with respect to the plane defined by the anthracene atoms C11–C12–C13–C14. Furthermore, the dithiolenyl rings are folded by 10–12° along the S...S axes.

Figure 12a summarizes the optimized values for selected bond lengths of **14**. The shortest bond lengths correspond to the carbon–carbon (CC) bonds of the dithiolenyl rings (1.34–1.35 Å) and to the exocyclic CC bonds linking the dithiolenyl rings to the anthracene units (1.36 Å). The outer benzene rings of these units present an aromatic structure since all the CC bonds have a length of (1.40 ± 0.01 Å).

To investigate the nature of the electronic transitions that give rise to the absorption bands observed in the experimen-

tal UV/Vis spectrum, the electronic excited states of **12** and **14** were calculated using the time-dependent DFT (TDDFT) approach and the B3P86/6-31G*-optimized geometries. TDDFT calculations were performed in acetonitrile solution at the B3P86/6-31G** level. Solvent effects were taken into account by using the polarized continuum model (PCM).

Calculations predict that the lowest energy absorption band, observed at 431 nm for **12** and at 436 nm for **14**, is as a result of the electronic transition to the first excited state calculated at 2.89 eV (429 nm) and 2.82 eV (439 nm), respectively. Calculations thus reproduce the small bathochromic shift measured in passing to the dimer. The electronic transition corresponds in both cases to the promotion of one electron from the HOMO to the LUMO and is computed to be more intense for the dimer (oscillator strength $f=0.46$ for **12** and 1.08 for **14**). As shown in Figure 13 for **12**, the

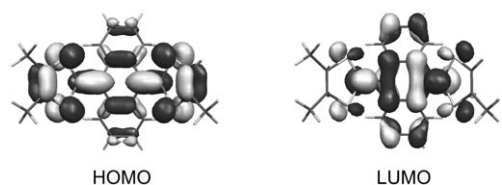


Figure 13. Electron density contours (0.03 e bohr^{-3}) calculated for the HOMO and the LUMO of **12**. Similar topologies are found for **14**.

HOMO→LUMO excitation implies some electron-density transfer from the dithiole rings, on which the HOMO is mainly located, to the anthracene units, on which the LUMO mainly spreads. Calculations therefore suggest that the first absorption band implies some intramolecular charge transfer.

TDDFT calculations indicate that the absorption band observed at 367 nm for **12** is due to the electronic transition calculated at 361 nm ($f=0.17$). The transition results from mixing of the HOMO-1→LUMO and HOMO→LUMO+1 one-electron excitations and also implies some electron-density transfer from the dithiole fragments to the anthracene units. The absorption band is also measured at 367 nm for **14**, but now it is associated with two transitions calculated at 365 nm ($f=0.25$) and 357 nm ($f=0.10$) due to the splitting of the molecular orbitals (MOs) in the dimer. The highest energy band, recorded at 238 nm for both **12** and **14**, is due to intense transitions that mainly involve the anthracene moiety [**12**: 235.4 nm ($f=0.57$); **14**: 236.2 nm ($f=0.40$), and 236.6 nm ($f=0.33$)]. The calculated vertical excitation energies are thus in good agreement with the experimental data and allow for a comprehensive assignment of the spectrum.

Oxidized compounds: The equilibrium geometries of the dication and tetracation of **14** were calculated under different symmetry restrictions to investigate how the oxidation process affects the molecular structure and the electronic prop-

erties of the molecule. The molecular geometries of **12**²⁺ and **12**²⁺ were also optimized at the B3P86/6-31G* level for comparison purposes. Similarly to that previously found for unsubstituted exTTF,^[3,22] **12**²⁺ preserves the butterfly-shaped structure of the neutral molecule, while **12**²⁺ adopts an orthogonal conformation in which the dithiole rings lie perpendicular to the central anthracene unit, which is fully planar.

The minimum-energy structure calculated for **14**²⁺ corresponds to a C_2 form, similar to that depicted in Figure 11b for the neutral molecule, in which both exTTF moieties exhibit a butterfly conformation. In this structure, the charge is equally shared by the two exTTF units and the geometry of these units is almost identical to that calculated for **12**²⁺. The structure therefore corresponds to a delocalized D^{2+} - D^0 species proposed experimentally, the structure of **14**²⁺ was built up by connecting the optimized geometries of **12**²⁺ (orthogonal conformation) and neutral **12** (butterfly conformation). Upon geometry relaxation, the exTTF moieties preserve different conformations but the positive charge becomes redistributed over the two moieties. A partially localized structure is therefore obtained, in which the orthogonal exTTF fragment supports a charge of +1.27e and shows bond lengths intermediate between those of **12**²⁺ and **12**²⁺, while the butterfly exTTF fragment has a charge of +0.73e and its bond lengths are similar to those of **12**²⁺. The optimized structure was calculated to be $9.16 \text{ kcal mol}^{-1}$ higher in energy than the fully-delocalized, butterfly-shaped C_2 structure.^[24]

Theoretical calculations therefore predict that the most stable structure of compound **14**²⁺ corresponds to a delocalized D^{2+} - D^0 species. This apparently contradicts the experimental results discussed above. Experiments indicate that oxidation to the dication undoubtedly leads to a localized D^{2+} - D^0 species, in which only one of the donor fragments has been oxidized. However, it should be taken into account that theoretical results are obtained for the isolated molecule while experimental data are recorded in solution.

To make the comparison between theory and experiment more reliable, the molecular structures of **14**²⁺ were re-optimized in the presence of the solvent (CH_3CN , dielectric constant $\epsilon=36.7$) using the PCM approach. The solvent does not significantly affect the structure of the delocalized D^{2+} - D^0 species; the maximum differences found for the bond lengths are only 0.002 \AA . In contrast, the solvent drastically influences the structure of the D^{2+} - D^0 form, which now actually corresponds to a localized species. As shown in Figure 14a, one of the exTTF units presents an orthogonal conformation, in which both the dithiole rings and the anthracene unit are fully planar, while the other exTTF unit exhibits a butterfly conformation. The structural differences between the two units are shown in Figure 12b, in which the lengths of selected bonds are given. The orthogonal unit supports a charge of +1.90e and the bond lengths are almost identical to those calculated for **12**²⁺. The butterfly

unit has a charge of +0.10e and the bond lengths correspond to those found for neutral compounds **12** and **14**. This charge-localized $D^{2+}-D^0$ structure is calculated to be 5.09 kcal mol⁻¹ more stable than the fully delocalized $D^{+}-D^{+}$ structure, in agreement with experimental observations.

Theoretical calculations therefore suggest that **14**²⁺ exists as a delocalized $D^{+}-D^{+}$ species in the gas phase and as a localized $D^{2+}-D^0$ species in solution. The interactions with the solvent favor the localization of the charge on one exTTF unit and stabilize the polarized $D^{2+}-D^0$ structure (dipole moment $\mu=46.1$ D). The influence of solvent polarity was studied by re-optimizing the structures of **14**²⁺ in a less-polar solvent like CH₂Cl₂ ($\epsilon=8.93$). The localized $D^{2+}-D^0$ structure continues to be more stable in CH₂Cl₂ by 2.32 kcal mol⁻¹, but it is slightly less polarized ($\mu=45.2$ D) owing to the lower polarity of the solvent.

The minimum-energy conformation calculated for the tetracation **14**⁴⁺ in CH₃CN solution corresponds to the C_2 structure ($D^{2+}-D^{2+}$) depicted in Figure 14b. In this struc-

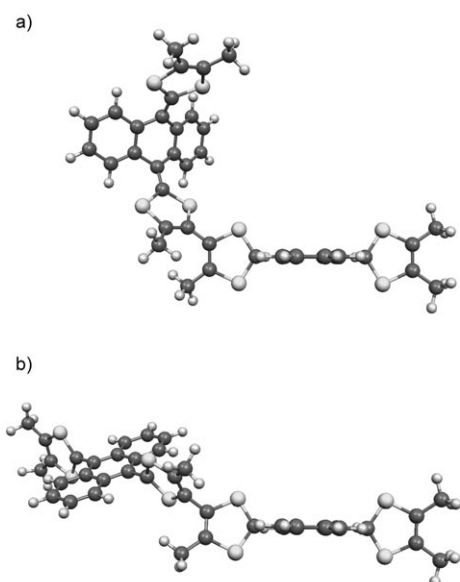


Figure 14. Minimum-energy B3P86/6-31G*-optimized conformations calculated for a) **14**²⁺ (no symmetry, in CH₃CN) and b) **14**⁴⁺ (C_2 symmetry, in CH₃CN).

ture, both exTTF units show a conformation typical of exTTF dications; the anthracene moieties are almost planar and the outer dithiole rings lie perpendicular to the anthracene planes. The inner dithiole rings are rotated by 106° around the central single bond to minimize the steric interactions and form an angle of 76° with the anthracene units. The C_{2h} conformation, in which the four dithiole rings lie in the same plane and are perpendicular to the two planar anthracenes, was also optimized at the B3P86/6-31G* level and it was found to be 2.70 kcal mol⁻¹ less stable than the twisted C_2 structure.

The bond lengths calculated for the anthracene units of **14**⁴⁺ (Figure 12c) are almost identical to those obtained for

the anthracene molecule in its neutral state (Figure 12d). This suggests that in **14**⁴⁺ the electrons have been mainly removed from the dithiole rings, while the anthracene units remain essentially neutral. The net atomic charges calculated using the natural population analysis (NPA) algorithm confirm this assumption. The dithiole rings accumulate charges of +0.93e (outer rings) and +0.88e (inner rings), while the anthracene units have a charge of +0.19e. The slightly smaller charges supported by the inner dithiole rings are due to the vicinity of these rings to each other, this increasing the Coulombic repulsion. The tetracation **14**⁴⁺ can, therefore, be visualized as two aromatic anthracene units (14 π electrons) substituted by singly charged dithiole rings (6 π electrons). Thus, the **14**⁴⁺ species consists of six aromatic, nearly orthogonally oriented π -subsystems (see Figure 14b).

We finally discuss the evolution of the optical properties upon oxidation. As shown in Figure 6b, the intense absorption band observed for **14** at 436 nm disappears as oxidation proceeds and a less-intense, broad band emerges in the 460–540 nm region. The new band is assigned to an electronic transition computed at 2.86 eV ($\lambda=434$ nm, oscillator strength $f=0.47$) for **14**⁴⁺. Calculations correctly predict the lower intensity of the band compared with the neutral molecule ($f=1.08$), but slightly underestimate its wavelength. The MOs involved in the transition (HOMO→LUMO+5, HOMO-1→LUMO+4) reside on the anthracene moieties and their atomic orbital (AO) composition reveals that it actually corresponds to the HOMO→LUMO transition of neutral anthracene. The nature of the lowest energy band of the electronic spectrum therefore changes upon oxidation. For neutral compound **14** it implies some charge transfer from the dithiole rings to the anthracene moieties, while for **14**⁴⁺ it only concerns the anthracene units. **14**⁴⁺ actually presents a series of low-energy transitions in the 1.6–2.8 eV range that involve electron promotions from the HOMO and HOMO-1, located on the anthracene units, to the lower unoccupied MOs (LUMO to LUMO+3), associated with the dithiole rings. All these transitions imply intramolecular charge transfers but they have very small or negligible intensities. Only those transitions involving the inner dithiole rings, that are not exactly perpendicular to the anthracene moieties, present an appreciable intensity ($f=0.01-0.02$) and could contribute to the lower energy side of the broad band observed experimentally.

Calculations show that the increase in the band at 258.5 nm upon oxidation (Figure 6b) is also related to the anthracene moieties. It is attributed to a very intense electronic transition ($f=1.43$) calculated at 4.96 eV (250 nm) for **14**⁴⁺. The transition actually corresponds to the HOMO→LUMO+1 excitation of neutral anthracene, which is experimentally observed at 4.92 eV.^[25] The electronic spectrum of the oxidized species **14**⁴⁺ is therefore dominated by the spectroscopic features of the anthracene moieties. Only the experimental band observed at 311 nm is assigned by calculations to electronic transitions associated with the inner (303 nm, $f=0.39$) and outer (293 nm, $f=0.43$) dithiole rings.

Conclusion

In summary, we have carried out the synthesis of a new exTTF dimer (**14**), in which, for the first time, the two exTTF units are covalently connected by the 1,3-dithiole rings. The close proximity between the 1,3-dithiole rings of both exTTF units results in a significant electronic interaction between them with a strong impact on the electrochemical properties and the electronic spectra. CV experiments in solution and under thin-layer conditions supported by electrochemical simulation and SEC measurements clearly show that the electrochemical oxidation of compound **14** occurs as two consecutive 2e processes $D^0-D^0 \rightarrow D^{2+}-D^0 \rightarrow D^{2+}-D^{2+}$. Theoretical calculations carried out by using the DFT approach (B3P86/6-31G*) give support to the experimental findings and confirm that oxidation of **14** leads to 14^{2+} which exists as a delocalized $D^{2+}-D^+$ species in the gas phase and as a localized $D^{2+}-D^0$ species in solution (either in CH_3CN or in the less-polar solution CH_2Cl_2). The tetracation 14^{4+} can be visualized as two aromatic anthracene units substituted by 1,3-dithiolium cations forming the $D^{2+}-D^{2+}$ species.

Experimental Section

9-(4-Iodo-5-methyl-1,3-dithiol-2-ylidene)-10-(4,5-dimethyl-1,3-dithiol-2-ylidene)-9,10-dihydroanthracene (13): Into a stirred solution of **12**^[7] (422 mg, 1.00 mmol) in dry tetrahydrofuran (100 mL) at $-78^\circ C$ under argon, lithium diisopropylamide (LDA) (1.18 mL, 1.50 mmol) was added dropwise over a period of 5 min. The reaction was stirred for 1 h at $-78^\circ C$ to give a thick yellow precipitate containing the anion. Into this suspension was syringed perfluorohexyl iodide (PFHI) (0.38 mL, 1.50 mmol) and stirring was continued at $-78^\circ C$ for a further 1 h, and then the mixture was allowed to reach $20^\circ C$ overnight. After evaporation of the solvent, the residue was diluted with water (50 mL) and extracted with dichloromethane (3 × 50 mL). The organic extracts were combined and washed sequentially with water (2 × 50 mL) and brine (1 × 50 mL), and then dried ($MgSO_4$). After removing the solvent in vacuo, the residue was purified by column chromatography on silica gel (eluent: hexane) to afford the product **13** as a yellow solid (455 mg, 83%); m.p. $210-212^\circ C$. Elemental analysis calcd (%) for $C_{23}H_{17}S_4$: C 50.36, H 3.12; found: C, 50.16, H, 3.12. MS (EI): m/z (%) 548 ($[M^+]$, 68), 421 ($[M^+ - I]$, 10); 1H NMR (300 MHz, $CDCl_3$): $\delta = 7.68-7.63$ (m, 2H; ArH), $7.57-7.48$ (m, 2H; ArH), $7.31-7.26$ (m, 4H; ArH), 2.04 (s, 3H; Me), 1.93 ppm (s, 6H; 2 Me); ^{13}C NMR (50 MHz, $CDCl_3$): $\delta = 135.3$, 135.2, 134.7, 134.6, 130.2, 126.1, 125.8, 125.6, 125.4, 125.1, 124.7, 123.3, 120.8, 18.9 (CH_3), 13.1 ppm ($2CH_3$); FTIR (KBr): $\nu = 2906$, 1512, 1444, 1283, 756, 675, 644, 497 cm^{-1} ; UV (CH_2Cl_2): $\lambda = 238$, 368, 437 nm.

Bis[9-(4,5-dimethyl-1,3-dithiol-2-ylidene)-10-(4-methyl-1,3-dithiol-2-ylidene)-9,10-dihydroanthracene] (14): Compound **13** (252 mg, 0.460 mmol) was dissolved in 1-methylpyrrolidin-2-one (NMP) (5.0 mL) under argon. Copper(I) thiophene-2-carboxylate (263 mg, 1.30 mmol) was added and the mixture was stirred for 2 days at room temperature, then diluted with ethyl acetate (100 mL). A solution of 15% aqueous ammonia was added until a clear blue aqueous layer had formed. This layer was extracted with ethyl acetate (3 × 50 mL). The organic extracts were combined and washed sequentially with water (2 × 100 mL) and brine (100 mL). The organic phase was dried ($MgSO_4$) and the solvent evaporated. The residue was chromatographed eluting with hexane/dichloromethane (9/1) affording compound **14** as a yellow solid (41 mg, 21%); mp $243-244^\circ C$. Elemental analysis calcd (%) for $C_{46}H_{34}S_8$: C, 65.52, H, 4.06; found: C, 65.72, H, 4.36. MS (EI): m/z (%) 842 ($[M^+]$, 8), 421 ($[M^{2+}]$, 100); 1H NMR

(300 MHz, $CDCl_3$): $\delta = 7.63-7.57$ (m, 8H; ArH), $7.28-7.25$ (m, 8H; ArH), 1.93 (s, 12H; 4 Me), 1.90 ppm (s, 6H; 2 Me); ^{13}C NMR (50 MHz, $CDCl_3$): $\delta = 135.3$, 134.9, 125.9, 125.8, 125.7, 125.4, 125.2, 124.9, 15.8 ($2CH_3$), 13.1 ppm ($4CH_3$); FTIR (KBr): $\nu = 2916$, 2850, 1585, 1522, 1458, 1444, 1280, 1261, 1093, 808, 754, 675, 644 cm^{-1} ; UV (CH_2Cl_2): $\lambda = 238$, 370, 442 nm.

Electrochemistry and spectroelectrochemistry: CV was performed in a three-electrode cell equipped with a platinum millielectrode (\varnothing 1.6 or 1.0 mm) and a platinum-wire counter electrode. For CV experiments in AN and DCM a nonaqueous Ag/Ag⁺ electrode (0.01 N AgNO₃ in dry AN) was used as the reference electrode. For CV experiments in AN:DCM a silver wire served as the quasireference electrode and its potential was checked against the ferrocene/ferricinium couple (Fc/Fc⁺) before and after each experiment. In both cases the potentials were then recalculated against Fc/Fc⁺, which showed the following potentials against the reference electrodes used: +0.078 V (vs. Ag/Ag⁺ in AN), +0.130 V (vs. Ag/Ag⁺ in DCM), +0.465 V (vs. Ag wire in AN:DCM, 1:1 v/v). CVs were recorded in AN, DCM, or a mixture of both (1:1 v/v) with tetrabutylammonium hexafluorophosphate (Bu_4NPF_6) as the supporting electrolyte. Experiments in AN and DCM were performed in dry HPLC-grade solvents, deoxygenated by bubbling Ar through the solution. All experiments in the AN:DCM mixture were performed in a glove box containing dry, oxygen-free (< 1 ppm) argon, at room temperature. Electrochemical experiments were carried out with an EGG PAR 273A potentiostat or a BAS-CV50W electrochemical workstation with positive feedback compensation. Based on repetitive measurements, absolute errors on potentials were found to be approximately ± 5 mV.

SEC measurements in AN and DCM were performed on a Varian Cary 5E spectrophotometer in a 1 mm quartz cell using a Pt grid as the working electrode and Pt wires as the counter and reference electrodes, with 0.1 M Bu_4NPF_6 as the supporting electrolyte. The setup for thin-layer SEC experiments (TL-SEC) in a reflection mode has been described previously.^[26] TL-SEC experiments in AN:DCM, 1:1 v/v were performed for thin-layer solutions ($\sim 125 \mu m$) with UV/vis-NIR spectra recorded in a reflection mode (reflection from a \varnothing 5 mm finely polished Pt disk) on a Lambda 19 NIR Perkin-Elmer spectrophotometer.

UV/Vis spectra of 12 and 14 oxidized with $NOSbF_6$: Chemical oxidation of compounds **12** and **14** with $NOSbF_6$ was performed in a spectrophotometric 1 mm quartz cell. Fixed aliquots of $NOSbF_6$ solution in AN were added repetitively to the solution of either **12** or **14** in AN by a syringe and the spectra were recorded on a Lambda 19 NIR Perkin-Elmer spectrophotometer. All solutions were prepared in a glove box containing dry, oxygen-free (< 1 ppm) argon at room temperature.

Computational details: All theoretical calculations were carried out within the DFT approach using the Gaussian 03 program package^[27] and the Becke's three-parameter B3P86 exchange correlation functional.^[28] The B3P86 functional has been recognized as providing equilibrium geometries for sulfur-containing compounds in better accord with experimental data and ab initio post Hartree-Fock (HF) calculations than the more widely used B3LYP functional.^[29] Geometry optimizations were performed by using the 6-31G* basis set.^[30] Vertical electronic excitation energies were determined by means of the TDDFT approach.^[31] Numerous hitherto reported applications indicate that TDDFT employing current exchange-correlation functionals performs significantly better than HF-based single-excitation theories for the low-lying valence excited states. TDDFT calculations were carried out using the 6-31G** basis set.^[32] Solvent effects were considered within the SCRf (self-consistent reaction field) theory using the PCM approach to model the interaction with the solvent.^[33] The PCM model considers the solvent as a continuous medium with a dielectric constant ϵ , and represents the solute by means of a cavity built with a number of interlaced spheres.^[34] Net atomic charges were calculated using the NPA analysis^[35] included in the natural-bond-orbital (NBO) algorithm proposed by Weinhold and co-workers.^[36]

Acknowledgements

The work in Durham and Madrid was funded by the ESF Eurocores SONS Programme, with additional support from EPSRC and BQU2002-00855. The work at Valencia was supported by the MEC of Spain and by FEDER funds (Grant BQU2003-05111). We thank N. Godbert for assistance with the initial synthesis of compounds **13** and **14**.

- [1] a) J. L. Segura, N. Martín, *Angew. Chem.* **2001**, *113*, 1416–1455; *Angew. Chem. Int. Ed.* **2001**, *40*, 1372–1409; b) N. Martín, E. Ortí, in *Handbook of Advanced Electronic Photonic Materials and Devices, Vol. 3* (Ed.: H. S. Nalwa), Academic Press, San Diego, **2001**, pp. 245–265; c) Y. Yamashita, in *TTF Chemistry. Fundamentals and Applications of tetrathiafulvalene*, (Eds.: J. Yamada, T. Sugimoto), Kodansha, Springer, Tokyo, **2004**, pp. 287–310; d) For recent reviews on TTF in materials and supramolecular chemistry see: M. R. Bryce, *J. Mater. Chem.* **2000**, *10*, 589–598; e) M. B. Nielsen, C. Lomholt, J. Becher, *J. Chem. Soc. Rev.* **2000**, *29*, 153–164; f) see also the special issue *Chem. Rev.* **2004**, *104*.
- [2] a) Y. Yamashita, Y. Kobayashi, T. Miyashi, *Angew. Chem.* **1989**, *101*, 1090–1091; *Angew. Chem. Int. Ed. Engl.* **1989**, *28*, 1052–1053; b) M. R. Bryce, A. J. Moore, M. Hasan, G. J. Ashwell, A. T. Fraser, W. Clegg, M. B. Hursthouse, A. I. Karaulov, *Angew. Chem.* **1990**, *102*, 1493–1495; *Angew. Chem. Int. Ed. Engl.* **1990**, *29*, 1450–1452; c) A. J. Moore, M. R. Bryce, *J. Chem. Soc. Perkin Trans. 1* **1991**, 157–168.
- [3] N. Martín, L. Sánchez, C. Seoane, E. Ortí, P. M. Viruela, R. Viruela, *J. Org. Chem.* **1998**, *63*, 1268–1279.
- [4] B. Insuasti, C. Atienza, C. Seoane, N. Martín, J. Garín, J. Orduna, R. Alcalá, B. Villacampa, *J. Org. Chem.* **2004**, *69*, 6986–6995, and references therein.
- [5] a) N. Martín, I. Pérez, L. Sánchez, C. Seoane, *J. Org. Chem.* **1997**, *62*, 5690–5695; b) N. Martín, L. Sánchez, D. M. Guldi, *Chem. Commun.* **2000**, 113–114; c) M. A. Herranz, N. Martín, L. Sánchez, C. Seoane, D. M. Guldi, *J. Organomet. Chem.* **2000**, *599*, 2–7; d) M. A. Herranz, B. M. Illescas, N. Martín, Ch. Luo, D. M. Guldi, *J. Org. Chem.* **2000**, *65*, 5728–5738; e) M. A. Herranz, N. Martín, J. Ramey, D. M. Guldi, *Chem. Commun.* **2002**, 2968–2968; f) S. González, N. Martín, A. Swartz, D. M. Guldi, *Org. Lett.* **2003**, *5*, 557–560; g) M. C. Díaz, M. A. Herranz, B. M. Illescas, N. Martín, N. Godbert, M. R. Bryce, Ch. Luo, A. Swartz, G. Anderson, D. M. Guldi, *J. Org. Chem.* **2003**, *68*, 7711–7721; h) S. González, N. Martín, D. M. Guldi, *J. Org. Chem.* **2003**, *68*, 779–791; i) L. Sánchez, I. Pérez, N. Martín, D. M. Guldi, *Chem. Eur. J.* **2003**, *9*, 2457–2468.
- [6] a) E. Cerrada, M. R. Bryce, A. J. Moore, *J. Chem. Soc. Perkin Trans. 1* **1993**, 537–538; b) G. J. Marshallsay, M. R. Bryce, *J. Org. Chem.* **1994**, *59*, 6847–6850.
- [7] a) M. R. Bryce, T. Finn, A. J. Moore, A. S. Batsanov, J. A. K. Howard, *Eur. J. Org. Chem.* **2000**, 51–60; b) N. Godbert, M. R. Bryce, S. Dahaoui, A. S. Batsanov, J. A. K. Howard, P. Hazendonk, *Eur. J. Org. Chem.* **2001**, 749–757; c) M. C. Díaz, B. M. Illescas, N. Martín, *Tetrahedron Lett.* **2003**, *44*, 945–948.
- [8] a) M. R. Bryce, A. S. Batsanov, T. Finn, T. K. Hansen, J. A. K. Howard, M. Kamenjicki, I. K. Lednev, S. A. Asher, *Chem. Commun.* **2000**, 295–296; b) D. F. Perepichka, M. R. Bryce, I. F. Perepichka, S. B. Lyubchik, C. A. Christensen, N. Godbert, A. S. Batsanov, E. Levillain, E. J. L. McInnes, J. P. Zhao, *J. Am. Chem. Soc.* **2002**, *124*, 14227–14238; c) F. Giacalone, J. L. Segura, N. Martín, D. M. Guldi, *J. Am. Chem. Soc.* **2004**, *126*, 5340–5341.
- [9] a) C. Bouille, O. Desmars, N. Gautier, P. Hudhomme, M. Cariou, A. Gorgues, *Chem. Commun.* **1998**, 2197–2198; b) N. Gautier, N. Mercier, A. Riou, A. Gorgues, P. Hudhomme, *Tetrahedron Lett.* **1999**, *40*, 5997–6000.
- [10] N. Gautier, N. Gallego-Planas, N. Mercier, E. Levillain, P. Hudhomme, *Org. Lett.* **2002**, *4*, 961–963.
- [11] I. Pérez, S.-G. Liu, N. Martín, L. Echegoyen, *J. Org. Chem.* **2000**, *65*, 3796–3803.
- [12] M. Iyoda, M. Hasegawa, Y. Miyake, *Chem. Rev.* **2004**, *104*, 5085–5113.
- [13] N. Martín, I. Pérez, L. Sánchez, C. Seoane, *J. Org. Chem.* **1997**, *62*, 870–877.
- [14] N. Godbert, M. R. Bryce, *J. Mater. Chem.* **2002**, *12*, 27–36.
- [15] M. C. Díaz, B. M. Illescas, C. Seoane, N. Martín, *J. Org. Chem.* **2004**, *69*, 4492–4499.
- [16] C. Christensen, M. R. Bryce, A. S. Batsanov, J. Becher, *Org. Biomol. Chem.* **2003**, *1*, 511–522.
- [17] C. Wang, A. Ellern, V. Khodorkovsky, J. Bernstein, J. Becker, *J. Chem. Soc. Chem. Commun.* **1994**, 983–984.
- [18] S. J. Zhang, D. W. Zhang, L. S. Liebeskind, *J. Org. Chem.* **1997**, *62*, 2312–2313.
- [19] K. Hu, D. H. Evans, *J. Electroanal. Chem.* **1997**, *423*, 29–35.
- [20] a) A. E. Jones, C. A. Christensen, D. F. Perepichka, A. S. Batsanov, A. Beeby, P. J. Low, M. R. Bryce, A. W. Parker, *Chem. Eur. J.* **2001**, *7*, 973–978; b) D. M. Guldi, L. Sánchez, N. Martín, *J. Phys. Chem. B* **2001**, *105*, 7139–7144; c) N. Martín, L. Sánchez, D. M. Guldi, *Chem. Commun.* **2000**, 113–114.
- [21] W. Koch, M. C. Holthausen, *A Chemist's Guide to Density Functional Theory*, Wiley-VCH, Weinheim, Germany, **2000**.
- [22] M. C. Díaz, B. M. Illescas, N. Martín, R. Viruela, P. M. Viruela, E. Ortí, O. Brede, I. Zilbermann, D. M. Guldi, *Chem. Eur. J.* **2004**, *10*, 2067–2077.
- [23] a) S. Triki, L. Ouahab, D. Lorcy, A. Robert, *Acta Crystallogr. Sect. C* **1993**, *49*, 1189–1192; b) M. R. Bryce, T. Finn, A. S. Batsanov, R. Kataký, J. A. K. Howard, S. B. Lyubchik, *Eur. J. Org. Chem.* **2000**, 1199–1205; c) C. A. Christensen, A. S. Batsanov, M. R. Bryce, J. A. K. Howard, *J. Org. Chem.* **2001**, *66*, 3313–3320.
- [24] The two structures were also optimized at the B3LYP/6-31G* level and an almost identical energy difference (9.32 kcal mol⁻¹) was obtained between them.
- [25] H. H. Perkampus, *UV-VIS Atlas of Organic Compounds*, Wiley-VCH, Weinheim, Germany **1992**.
- [26] F. Gaillard, E. Levillain, *J. Electroanal. Chem.* **1995**, *398*, 77–87.
- [27] M. J. Frisch, G. W. Trucks, H. B. Schlegel, G. E. Scuseria, M. A. Robb, J. R. Cheeseman, J. A. Montgomery, T. Jr., Vreven, K. N. Kudin, J. C. Burant, J. M. Millam, S. S. Iyengar, J. Tomasi, V. Barone, B. Mennucci, M. Cossi, G. Scalmani, N. Rega, G. A. Petersson, H. Nakatsuji, M. Hada, M. Ehara, K. Toyota, R. Fukuda, J. Hasegawa, M. Ishida, T. Nakajima, Y. Honda, O. Kitao, H. Nakai, M. Klene, X. Li, J. E. Knox, H. P. Hratchian, J. B. Cross, C. Adamo, J. Jaramillo, R. Gomperts, R. E. Startmann, O. Yazyev, A. J. Austin, R. Cammi, C. Pomelli, J. W. Ochterski, P. Y. Ayala, K. Morokuma, G. A. Voth, P. Salvador, J. J. Dannenberg, V. G. Zakrzewski, J. M. Dapprich, A. D. Daniels, M. C. Strain, O. Farkas, D. K. Malick, A. D. Rabuck, K. Raghavachari, J. B. Foresman, J. V. Ortiz, Q. Cui, A. G. Baboul, S. Clifford, J. Cioslowski, B. B. Stefanov, G. Liu, A. Liashenko, I. Piskorz, I. Komaromi, R. L. Martin, D. J. Fox, T. Keith, M. A. Al-Laham, C. Y. Peng, A. Manayakkara, M. Challacombe, P. M. W. Gill, B. G. Johnson, W. Chen, M. W. Wong, C. Gonzalez, J. A. Pople, *Gaussian 2003, Revision C.02*; Gaussian Inc.: Pittsburgh PA, **2003**.
- [28] J. P. Perdew, *Phys. Rev. B* **1986**, *33*, 8822–8824.
- [29] a) P. M. Viruela, R. Viruela, E. Ortí, J.-L. Brédas, *J. Am. Chem. Soc.* **1997**, *119*, 1360–1369; b) R. Liu, X. Zhou, H. Kasmai, *Spectrochim. Acta, Part A* **1997**, *53*, 1241–1256; c) J. A. Altmann, N. C. Handy, V. E. Ingamells, *Mol. Phys.* **1997**, *92*, 339–352.
- [30] P. C. Hariharan, J. A. Pople, *Chem. Phys. Lett.* **1972**, *16*, 217–219.
- [31] a) E. Runge, E. K. U. Gross, *Phys. Rev. Lett.* **1984**, *52*, 997–1000; b) E. K. U. Gross, W. Kohn, *Adv. Quantum Chem.* **1990**, *21*, 255–291; c) E. K. U. Gross, C. A. Ullrich, U. J. Gossmann, in *Density Functional Theory* (Eds.: E. K. U. Gross, R. M. Dreizler), Plenum Press, New York, **1995**; pp. 149–171; d) M. E. Casida, in *Recent Advances in Density Functional Methods, Part I* (Ed.: D. P. Chong), World Scientific, Singapore, **1995**; pp. 155–192.
- [32] M. M. Francl, W. J. Pietro, W. J. Hehre, J. S. Binkley, M. S. Gordon, D. J. Defrees, J. A. Pople, *J. Chem. Phys.* **1982**, *77*, 3654–3665.

- [33] a) J. Tomasi, M. Persico, *Chem. Rev.* **1994**, *94*, 2027–2094; b) C. S. Cramer, D. G. Truhlar, in *Solvent Effects and Chemical Reactivity* (Eds.: O. Tapia, J. Bertrán), Kluwer, Dordrecht, **1996**; pp. 1–80.
- [34] a) S. Miertus, E. Scrocco, J. Tomasi, *Chem. Phys.* **1981**, *55*, 117–119; b) S. Miertus, J. Tomasi, *Chem. Phys.* **1982**, *65*, 239–245; c) M. Cossi, V. Barone, R. Cammi, J. Tomasi, *Chem. Phys. Lett.* **1996**, *255*, 327–335; d) E. Cancès, B. Mennucci, J. Tomasi, *J. Chem. Phys.* **1997**, *107*, 3032–3041; e) V. Barone, M. Cossi, J. Tomasi, *J. Comput. Chem.* **1998**, *19*, 404–417; f) M. Cossi, G. Scalmani, N. Rega, V. Barone, *J. Chem. Phys.* **2002**, *117*, 43–54.
- [35] a) A. E. Reed, F. Weinhold, *J. Chem. Phys.* **1983**, *78*, 4066–4073; b) A. E. Reed, R. B. Weinstock, F. Weinhold, *J. Chem. Phys.* **1985**, *83*, 735–746.
- [36] A. E. Reed, L. A. Curtiss, F. Weinhold, *Chem. Rev.* **1988**, *88*, 899–926.

Received: August 16, 2005
Published online: January 23, 2006